Supplemental Materials of Paper "Dependable Structural Health Monitoring Using Wireless Sensor Networks"

Md Zakirul Alam Bhuiyan, *Member, IEEE*, Guojun Wang, *Member, IEEE*, Jie Wu, *Fellow, IEEE*, Jiannong Cao, *Fellow, IEEE*, Xuefeng Liu, *Member, IEEE*, and Tian Wang, *Member, IEEE*

APPENDIX A
EXTENDED ENERGY COST MODEL (COST(e_i))

One of our important objectives is to minimize the energy cost of the network regarding various aspects, including the sensor fault detection and recovery, damage event detection. Let $cost(e_i)$ denote the total energy cost of sensor i, including measurement, computation, transmission, and overhead. The sensor i has discrete power level that it can adjust it in ranges from $R_{\min}$ to $R_{\max}$. In the beginning, sensor i adopts its minimum power level and then i may dynamically increase it.

We describe here how energy consumed in transmitting a packet. The maximum energy cost of i depends on the routing protocol used by the data collection application. Consider a shortest path routing model [1], [2]; there is a path from sensor i to neighboring sensor node or the BS j: $q = z_0, z_1 \dots z_k$. Sensor i propagates the data to them. We can find the ith hop sensor on each path and calculate the amount of traffic that passes along on the paths within each round of monitoring data collection (T_d, d=1,2,…, n). Then, the $cost(e_i)$ can be decomposed into the following four parts:

$$\text{cost}(e_i) = e_T + e_{comp} + e_{samp} + e_{oh} \tag{A1}$$

We describe these terms in the following:

- e_T is the total energy cost for data transmission in a round of data transmission over a link between a transmitter and a receiver, where sensor i uses its power level from a minimum to a maximum, but not beyond the maximum power. We use a standard energy cost model for calculating the packet transmission cost [3].
- e_{comp} is the energy cost for processing data locally, e.g., computing equation (6) in Section 4.2. If a sensor is allowed to transmit the raw vibration data to the BS directly, e_{comp} would be very low. The cost is mainly due to the onboard processor, such as a micro-controller, DSP chip, or FPGA [4]. These devices consume energy proportional to the number of processing cycles, as well as the maximum processor frequency f, switching capacitance μ, and hardware specific constants k and β, respectively [4]. We focus on the number of cycles taken for tasks, e.g., equation (6) and the amount of samples taken. The number of cycles required to perform a task on the amount of samples (denoted by w) are estimated according to the computational complexity $O(w)$, which describes how many basic operations, i.e., averages, additions, multiplications, etc., must be performed in executing the task. Given these parameters, the computational energy to complete a task can be calculated according to:

$$e_{comp} = O(w) \cdot \mu(\frac{f}{k} + \beta) \tag{A2}$$

- e_{samp} is the energy required for a sampling cost of M data points; when sensors capture vibration signals, assuming a maximum 50% overlapping, $M = (n_a/2 + 1/2) \cdot c_r$, where n_a and c_r are the number of averages mainly for the purpose of noise reduction, that practically ranges from 10 to 20 and cross-correlation factor, respectively [5], [6]. We assume that n_a and c_r are set by fixed values on a sensor.
- e_{oh} is any additional overhead for some causes, e.g., fault detection and signal reconstruction, copying data to a local buffer, and network latency.

APPENDIX B
METHOD OF EXTRACTING LOCAL MODE SHAPE

In Section 4.2, we have described the state-space model for structural mode shape computation (Φ) at individual sensor. Here, we show a method to local Φ extraction and explain benefits of utilizing the extracted Φ over f towards sensor fault detection and tolerance.

- *M. Z. A. Bhuiyan is with the School of Information Science and Engineering, Central South University, Changsha, China, 410083, and Department of Computer and Information Sciences, Temple University, Philadelphia, PA 19122. E-mail: zakirulalam@gmail.com.*
- *G. Wang is with the School of Information Science and Engineering, Central South University, Changsha, China, 410083. E-mail: csgjwang@gmail.com (Corresponding Author).*
- *J. Wu is with the Department of Computer and Information Sciences, Temple University, Philadelphia, PA 19122. E-mail: jiewu@temple.edu.*
- *J. Cao and X. Liu are with the Department of Computing, The Hong Kong Polytechnic University, Hong Kong. E-mail: {csjcao,csxfliu}@comp.polyu.edu.hk.*
- *T. Wang is with the College of Computer Science and Technology, Huaqiao University, Xiamen, China, 361021. Email: wsnman@gmail.com.*

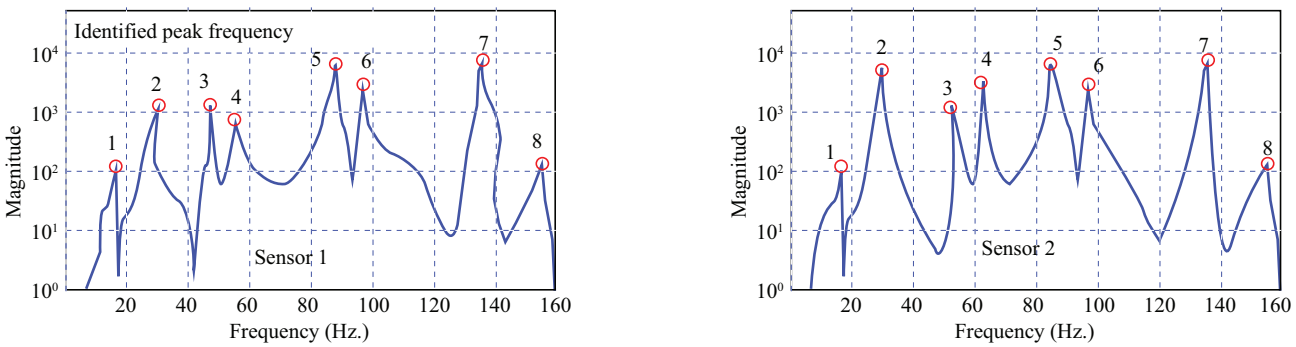

Fig. C1. Based on acquired vibration signal characteristics, measured natural frequencies captured by sensor 1 and sensor 2 under manual input excitation on the structure, respectively. This shows the structural system oscillation (moving back and forth) between its original state and its displaced state, captured by the two in their vicinity.

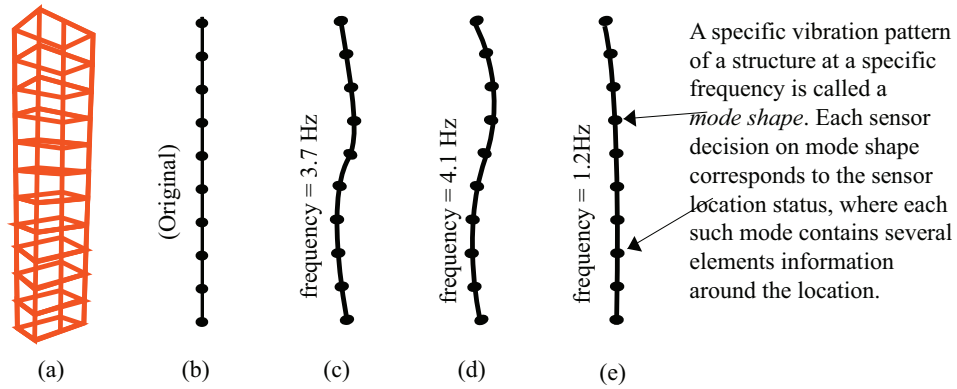

Fig. C2. (a) The finite element model (FEM) of our designed physical infrastructure; (b) its original mode shape; (c)-(e) its three mode shapes: mode 1, mode 2, and mode 3. *FEM* is a computer based numerical model often used for calculating the behavior and strength of structural mechanics, such as vibration and displacement.

Definition C1 [Natural Frequency]. *Every structure has a tendency to vibrate with much larger amplitude at some frequencies than others. Each such frequency is called a natural frequency denoted by f. f is an internal vibration signal characteristic of structure, and is different for different structures (such as from building to bridge, from indoor to outdoor). In other words, it is defined as the number of times that a structural system oscillates (moves back and forth) between its original state and its displaced state when assuming there is no outside interference.*

Definition C2 [Mode shape]. *When subjected to external forces, the response of a structure is conceptually similar to the response of a vibrating string or structural components such as a metal plate. Upon excitation, the vibrations are a combination of several harmonics (or at a specific frequency of vibrations), known as modes. Each mode deforms the structure into a particular spatio-temporal pattern known as a mode shape, denoted by Φ.*

B.1 Local Mode Shape by Each Sensor

As the network modeled in Section 3.1, m sensors are available for deployment on a structure, and they extract a total of p mode shapes from the measurement of m sensors. The corresponding natural frequencies and mode shapes are represented, respectively, as follows:

$$\mathbf{f} = [f^1, f^2, \ldots, f^p] \tag{B1}$$

$$\Phi = \begin{bmatrix} \Phi^1 & \Phi^2 & . & \Phi^m \end{bmatrix} = \begin{bmatrix} \phi_1^1 & \phi_2^1 & . & \phi_p^1 \\ \phi_1^2 & \phi_2^2 & . & \phi_p^2 \\ . & . & . & . \\ \phi_1^m & . & \phi_2^m & . & \phi_p^m \end{bmatrix} \tag{B2}$$

where $f^k (k = 1, \ldots, p)$ is the k^{th} natural frequency, Φ^k is the mode shape corresponding to $f^k \cdot \phi_i^k (i = 1, \ldots, m)$ is the value of Φ^k at the i^{th} sensor. For example, Fig. C1 and Fig. C2 illustrate the first two sensors' natural frequencies and corresponding mode shapes of a physical structure, receptively, which are extracted from measurements of 10 deployed sensors in our prototype system. In the experiment, vertical accelerations at all the given sensors are obtained, and 10% noise is added to all measurements. Under the artificial input excitation, the measured accelerations (the peak frequency pointed by $1, 2, \ldots$) at sensors 1 and sensor 2, respectively, refer

to Fig. C1 and Fig. C2 (which are obtained by using network topology in Fig. 3).

B.2 Φ over f in Sensor Fault Detection

The difference between f and Φ can be observed by comparing (C1) with (C2) and Fig. C1 with Fig. C2. According to the ACSM theory, f is not suitable characteristic for damage event detection due to several reasons:

(i) f is not a sensitive indicator to damage event, where only severe damage event causes noticeable change on the set of f;
(ii) Due to the global property, f does not contain any spatial information, and thus localizing damage event is difficult, while damage event detection using f is computationally inefficient;
(iii) High frequency modes are more susceptible to additional noise than low frequency modes; iv) f is susceptible to additional noise [6]; To improve the usability of the f to detect damage event of small magnitude, high-frequency modes, which are associated with local responses, may be used. However, we argue that adopting f is not suitable for WSNs considering WSNs' resource limitation;
(iv) Importantly, a large set of f is required to be sent to the BS (e.g., SPEM [2], NFMC [5]); damage event detection is greatly affected if a portion of it is lost during transmission.
(v) Φ is directly linked to topology of the structure and Φ highly features the dynamics of the structure.

On the other hand, it can be seen from (C2) that Φ has elements corresponding to each sensor, thus containing spatial information. Φ and its derivatives have been proven to be very sensitive features to detect damage event. It takes into account out-of-frequency-bandwidth modes of the structure, and is also applicable to a complex linear structure. This is why we target on Φ computation and observe the impact of sensor faults on Φ. However, theoretically, Φ is a global parameter of a structure which means that, using sensor deployed on different locations of a structure, the same set of Φ may not be obtained. To mitigate this problem, we allows each sensor estimate Φ taking measurements about its vicinity (i.e., local structural response).

In this paper, we utilize the mode shape curvature method proposed by civil engineering to identify significant change (i.e., damage event) in the mode shape [7]. The mode shape curvature has high sensitivity to damage event.

APPENDIX C
THE REASON OF NEGLECTING DAMPING

In Section 4.2, we have described the space-space model for the structural response measurements by sensors. In (6), we have considered the matrices of mass and stiffness coefficients of the various elements of the structure, but we have neglected the damping.

Damping is neglected in the model (6), considering individual sensor measurement estimation. In any case, (a) faults in the sensors will only be identified if they cause changes in the response of a greater magnitude than the errors in the estimated mode shape, and (b) the modes with low damping, having approximately real modes, will be strongly excited. Thus, undamped mode shapes can be accurately estimated by (6) at each sensor.

APPENDIX D
THE STATE-SPACE-EQUATION BASED KF FOR SIGNAL ANALYSIS

In Section 6, we proposed the Kalman filter (KF) technique for signal reconstruction. In this Appendix, a graphical representation of the state-space equation based KF is presented in Fig. D. This equation is made with the help of the state-space representation of the structural system, as described in Section 6.1. In Fig. D, u_t is the structural excitation at a specific frequency at time t. M_t and K_t are transition matrices. The signals σ_{t-1} and σ_t represent the measurement noises, respectively. When measuring the responses of a dynamical structural system by wireless sensors, the actual signals produced by the sensors are contaminated by noises due to internal manufacturing defects, physical interference, or external environmental effects. According to features of the KF, we assume that every measurement from the wireless sensors contains noises; thus, if the noise measurement is zero, the KL collapses. Setting the mean of noise as zero is a common practice: $E[\sigma_t] = 0$. Noises are assumed to be independent of each other, and are normally distributed with covariance matrices, $c_v = [\sigma\sigma^T]$. The underlying KF information is that KF is a recursive algorithm consisting of a loop, which is passed through for each time instant t.

APPENDIX E
MISSING SENSOR DETECTION METHOD

In Section 5, we presented Algorithm 2 for faulty sensor detection. However, if a sensor is missing or is out of service during the monitoring operation, if the sensor cannot be reached because of communication constraint or failure, or there is an unknown reason, the algorithm cannot guarantee detection of such a sensor node. In order to detect these sensors, we apply a method of Kullback-Leibler divergence (KL) [8] between the measured and estimated sensor signals and update Kalman filter (KF) with KL, which can be used as a fault indicator $\lambda_{n_i}^{KL-KF}$ KL-KF (Kullback-Leibler-Kalman-Filter) for such sensors. Note that for a faulty sensor signal reconstruction, we will use the Kalman filter (KL) technique.

The symmetrized form of the KL between the probability distributions of one measured signal (y_i) at time t and with the KF estimated signal $\hat{y}_i$ is as follows:

$$KL = \frac{1}{2}\sum_i [p_{y_i} - p_{\hat{y}_i}]\log_2 \frac{p_{y_i}}{p_{\hat{y}_i}} \quad \text{(E1)}$$

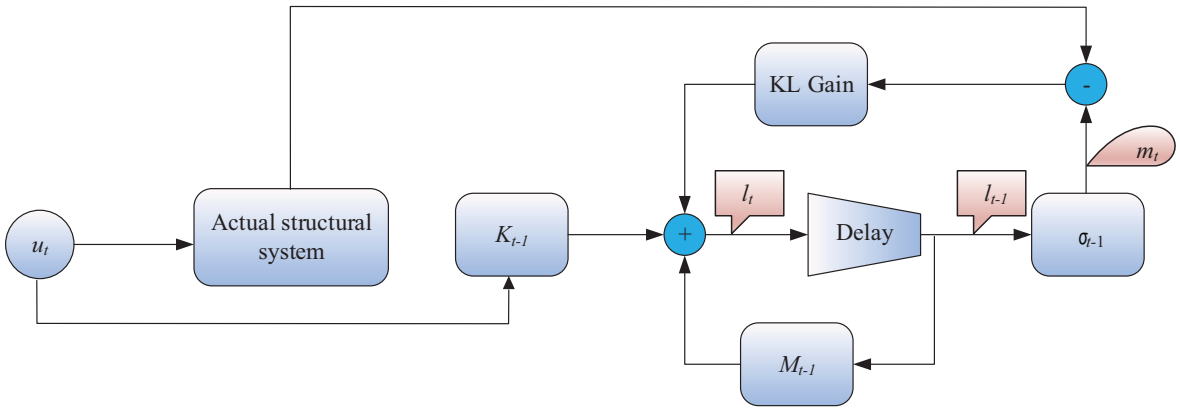

Fig. D. Graphical representation of the state-space equation based Kalman filter that is used in sensor's faulty signal reconstruction.

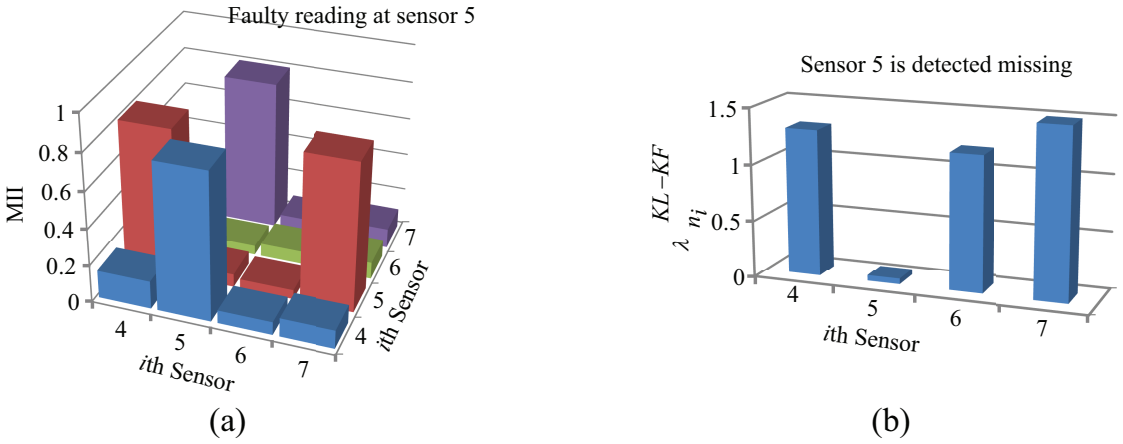

Fig. E. Missing or failed node detection in a WSN-based system: (a) an example of MII change in the sensor signals; (b) the detection result under the KL-KF.

where p_{y_i} is the probabilities based on the number of points falling into the ith bin. When the KL between two probability distributions is zero, the signals are identically distributed. The fault indicator is defined as:

$$\lambda_p^{KL-KF} = \frac{1}{p_{\max}-1}\sum_{p=1}^{p_{\max}} KL_p, 1 < p < p_{\max} \qquad \text{(E2)}$$

If the faulty sensor p is not used for the estimation of the p_{max} sensor signals, then the KL distance between the measured and estimated signals will be minimal; otherwise, the distance will be higher. This is shown under the network topology in Fig. 3a. It can be seen in Fig. D that without sensor 5, the best estimation is possible, which clearly indicates the sensor is faulty. This method based on KF is able to detect a missing or failed sensor. Also, pure bias faults with the MII method are enhanced further by this KL-KF method. Thus, using KF-KL with the help of Algorithm 2, it can be guaranteed to detect the fault types that produce faulty readings.

We illustrate the justification of sensor fault identification method based on MII (i.e., ω) through Algorithm 2. In our real experiment, under the manual random excitation and 5th sensor removal, the 5th sensor is detected as faulty. As shown in Fig. E(a), the relative change in MII indicates the sensor 5 as faulty. Actually, the sensor was removed from the location, however, the sensor is detected as missing by λ_p^{KL-KF}, as shown in Fig. E(b). To guarantee a certain redundancy of information in each sensor data set, the initial frequency should be available for identifying the faulty vibration signal. Therefore, if one of the neighboring nodes is missing, the KL-KF divergence between the measured and estimated sensor signals can be used as a sensor fault indicator.

APPENDIX F
MORE RESULTS OF WSN-BASED SHM SYSTEM DEPENDABILITY

In Section 7.1.2, we have partly performed an analysis of the system dependability. In the analysis, we have used a combination of true positive and true negative results in the sensor fault detection accuracy estimation. In this Appendix, we continue the analysis of the performance of the system dependability. We particularly consider the dependability of WSN-based SHM schemes as the ability

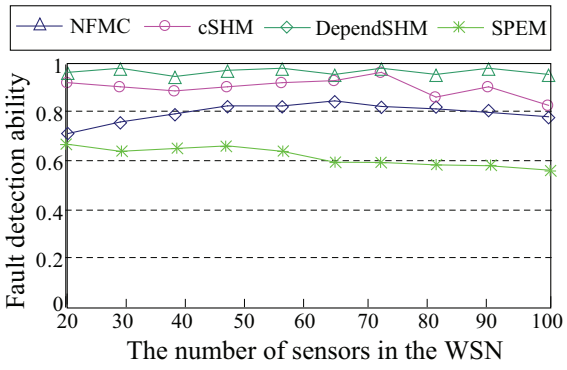

Fig. F1. Dependability verification: fault detection ability of different schemes.

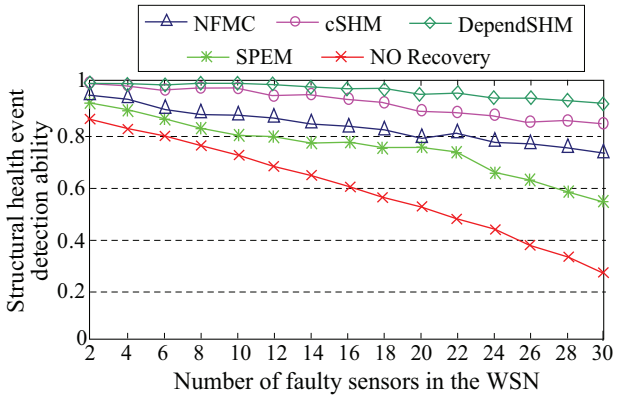

Fig. F2. Dependability verification: structural health event detection ability of different schemes.

of fault detection and the ability of structural health event (damage) detection of the schemes.

At first, we discuss the detection ability of different WSN-based schemes. Fig. F1 demonstrates the fault detection ability of `DependSHM` and other schemes. We can see that the detection ability of `DependSHM` is much better than that of cSHM, NFMC, and SPEM. NFMC shows higher detection errors than `DependSHM`, even higher than cSHM. Looking into details of causes, we summarize the following observations under the random fault injection:

(i) The same pick frequencies cannot be achieved in many neighborhoods or clusters in NFMC;
(ii) One or more clusters are disconnected from the network, as one or more faulty sensors are isolated based on the natural frequency comparison (although it shows the good ability rate of fault detection in some clusters);
(iii) The scheme is limited to the frequency matching based fault detection;
(iv) NFMC fails to detect other types of faults;
(v) The fault detection ability of SPEM is very low, due to non-faulty reading losses that results in a increased amount of faulty readings;
(vi) When attempting to recover from the faults, both SPEM and NFMC schemes require a significant amount of energy cost.

We next examine the system dependability in terms of the structural health event detection ability of a system. This can provide us an implication that how much a system can cope with sensor faults and what is the significance of addressing dependability issue in a system. We gather all the false positive and false negative cases appeared in the WSN-based SHM (achieved from a total of 50 simulation runs), and we get an average. Then, we calculate the structural health event detection ability rate as 1-(false positive rates + false negative rates). The results is depicted in Fig. F2. We also take into account the structural health monitoring under *NO* recovery (a preliminary analysis has been done based on these results, as illustrated in Fig. 8). Here, we intend to find evidence that what exactly happens when there is *NO* dependability option (fault detection and recovery) provided.

In Fig. F2, we can see the results, which shows that the structural event detection ability of `DependSHM` is between 93% and 97.2%, which greatly outperforms others. In SPEM, the detection ability under recovery from sensor faults tolerance algorithm is inferior (between 75% and 92%) among all of the schemes, while it is between 74% and 95% in NFMC and 87% to 95% in cSHM. There can be various reasons that SPEM provides poor detection rate, including i) centralized decision making on the fault detection and tolerance (data losses on the fly is a factor), ii) application-specific sensor deployment, iii) natural frequency matching problem, and so on. In NFMC, the peak natural frequency signals used in the sensor fault detection and recovery, by which the actual mode shape curvature slightly distorted. This lead to a lower MII that results in a lower structural event detection ability. As it can be seen in Fig. F2, the structural event detection ability becomes lower in NFMC and SPEM than in `DependSHM` and cSHM, as the number of faulty sensor nodes in the WSN increases.

From the results in Fig. F2, the structural event detection ability rate is around 65% in a system with *NO* recovery from sensor faults. It may make us surprised that the monitoring operations in a WSN-based SHM can be often meaningless if there is no dependability option provided. From a deep observation, we have found evidence that faulty sensors can corrupt results of a health event in a structural system without being detected. We have seen that measured signals introduced by some faulty sensors often identify its location as damaged (actually it is undamaged location). We also have found that some faulty sensor identify its location as undamaged (actually the location is damaged). There are a large number of such wrong diagnoses (false positive and false negative) that lead to a reduced structural event detection ability.

APPENDIX G
MORE DETAILS OF THE WSN PROTOTYPE SYSTEM IMPLEMENTATION

G.1 Extended Detail of the Experimental Setup

We validate DependSHM by implementing a proof-of-concept system using the TinyOS on Imote2 platforms [9]. Our main objective is to verify i) the dependability and ii) the energy-efficiency of the system. We target the accuracy or successful Φ identification, because it can provide us with the answer, whether or not a WSN-based SHM system is dependable in terms of various sensor faults.

The Imote2 (IPR2400) is an advanced wireless sensor platform (off-the-shelf), offering sufficient processing capability and communication resources to locally and continuously monitor vibration characteristics under intensive conditions. Its main board combines a low power PXA271 XScale processor with an 802.15.4 radio (CC2420) and an antenna using 2.4 GHz. The major limitation with it is the energy.

We employ 10 integrated Imote2s called SHM motes on a test structure, as shown in Fig. G1; an additional Imote2 is located 15 meters away as the BS mote, and a PC as a command center for the BS mote and data visualization. The test structure has 10 floors; at each floor, a mote is deployed to monitor the structure's horizontal accelerations. Each mote runs a program (implemented in the nesC language) to process the acceleration data acquired from on-board accelerometers. The BS receives the data packets from the sensors through wireless communication, and relays the data to the PC over a USB cable. The PC commands and sets parameters for the network through BS. Java and Matlab are used to calculate and visualize the whole structural health condition. In the experiment, R_{min} is adjusted by the diameter of the structure, which is adjusted by estimating the height of the test structure and each floor. Imote2's discrete levels of range are set to use R_{min} and R_{max}.

G.2 Sensor Identified Natural Frequencies

In Section 7.2.2, we have given experimental mode shapes, estimated based on natural frequencies. In the first set of experiments, we compute the natural frequencies, as shown in TABLE G1. These frequencies are used in creating mode shapes (Φ) in the base-line structural system, when there are no damage events and no sensor faults. Note that such a base-line mode shape should be not fixed but should be dynamic, i.e., a WSN-based SHM system can be enabled to adapt or update its base-line mode shape, taking into account dynamic environments and environmental noise factors. We find that the MII in different frequencies identified at different sensors is low (the result has been shown in Fig. 11).

G.3 Signal Reconstruction at a Faulty Sensor

In Section 7.2.2, we have also provided the sensor fault detection results, where we have found that sensor 5 is

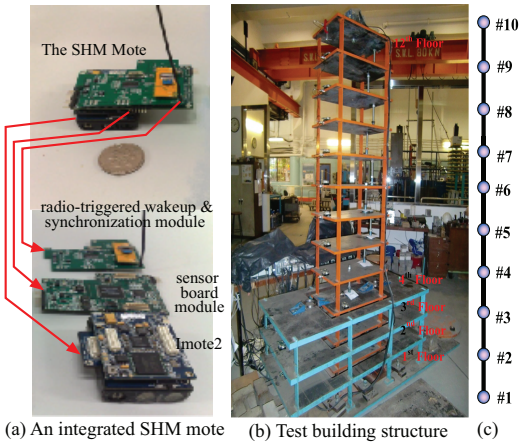

(a) An integrated SHM mote (b) Test building structure (c)

Fig. G1. (a) The SHM mote integrated by Imote2; (b) twelve-story test structure and the placement of 10 SHM motes on it; (c) their deployment.

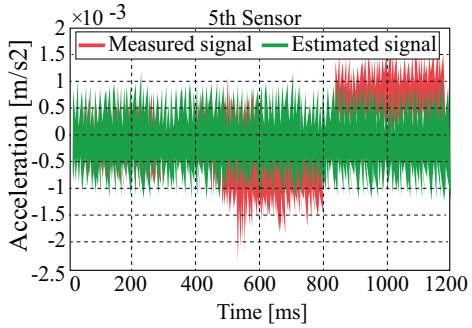

Fig. G2. Signal reconstruction of the 5th sensor (that is detected faulty).

faulty. In order to the support the results, we hereby can observe the faulty signal reconstruction of the 5th sensor, as shown in Fig. G2. The drift in the measured signal (red line) is corrected by the estimated signal (green lines). We observe the mutual independence under the fault injection at the 5th sensor. In DependSHM, when sensor nodes process data locally, the small value in the MII is achieved, ranging from 2% to 4%, and they are not considered faulty. The MII provides the best value, when there is a remarkable change in the sensor measured signals, i.e., the 5th sensor and 10th sensor are faulty. This reveals that there can a better accuracy of fault detection in DependSHM in practice, compared to others.

G.4 Energy Cost $(cost(e_i))$

Due to space limitation, we have not presented the performance of energy cost of the WSN in Section 7.2.2, which we present in this Appendix.

We allow all of the sensors to sleep after each monitoring period to perform power management. The TinyOS 2.0 drivers for the Imote2 supports putting all of the hardware to sleep when it is switched off. This is obvious for a WSN-based SHM system, since a WSN does not always need to run actively in case of specific structural

TABLE G1
Identified natural frequencies by the first five sensors of the experimental WSN in SPEM and DependSHM.

Mode	Frequencies (Hz)									
	Centralized processing (SPEM)					Localized processing (DependSHM)				
	s_1	s_2	s_3	s_4	s_5	s_1	s_2	s_3	s_4	s_5
1	13.211	12.213	14.131	15.123	13.435	14.134	13.141	15.312	16.856	14.355
2	17.341	14.798	15.112	16.234	15.141	17.741	15.141	17.214	17.852	16.641
3	20.834	21.334	19.134	21.434	19.746	21.341	22.932	21.341	22.344	21.341

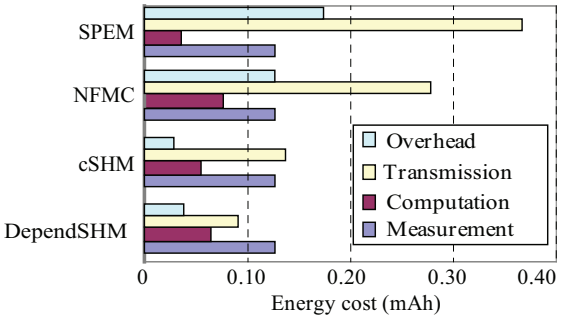

Fig. G3. The performance on the energy cost of the WSN in different schemes.

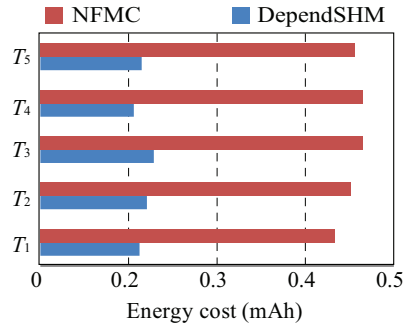

Fig. G4. The performance on the energy cost of the WSN in the first five round of monitoring in `DependSHM` and NFMC.

event monitoring. For example, in case of aerospace vehicle monitoring, when it is not flying, the WSN may not need monitoring operations. In another case, the WSN can be scheduled to run periodically or a part of the sensors can be scheduled to wake up periodically and check health event status. $cost(e_i)$ is calculated by the energy cost for computation, transmission, measurement, and overhead, where the overhead statistics with current cost data is combined. The data sheet can be found in [9].

Fig. G3 shows the energy cost of a round of monitoring, $T_{d=1}$. The `DependSHM` method significantly decreases the energy cost compared to SPEM, from 0.197 mAh to 0.072 mAh. The reason is that the major energy is consumed by the raw signal transmissions to the BS. The actual computation cost in `DependSHM` is 0.0072 mAh to execute the basic equations and fault detection and signal reconstitution. However, it fully depends on the number of cycles that a sensor CPU requires. It also varies from sensor to sensor based on the tasks a needs to do. A sensor does not need computation for signal reconstruction if there is not fault. In such a case, a sensor can save an average of 0.0027 mAh. More importantly, in `DependSys`, the computation saves the Imote2 an average of 0.165 mAh during transmission, since it reduces the time that the CC2420 radio is active. The overhead is caused by end-to-end transmission delay and writing/reading data to/from Imote2's memory, since we depend on local processing. In both SPEM and NFMC methods, transmitting a large amount of raw data in each T_d (i.e., transmission of natural frequency sets and frequent retransmissions caused by packet losses) increases $cost(e_i)$. However, NFMC achieves slightly lower energy cost for transmission than SPEM.

Further performance analysis of $cost(e_i)$ in five rounds of monitoring ($T_d, d = 1, ..., 5$) can be seen in Fig. G4. This shows the actual amount of energy cost required in `DependSHM`. We can see that `DependSHM` outperforms NFMC significantly because of the above causes, cluster maintenance, and network maintenance (e.g., faulty sensor isolation), particularly the set of mode shapes transmitted from the cluster-head to the BS. This is because the final mode shapes of each cluster is transmitted by each cluster-head, while SPEM requires transmission of all natural frequency sets. In our distributed solution, there is no frequent retransmission and the final mode shapes transmitted by each sensor are without sensor fault information. In the case of faulty sensor detection and signal reconstruction, the system consumes a small amount of energy in computation with a slight overhead, which is 5% to 8% of the total energy cost in each round.

In a concluding remark about the results we have found and presented in this paper, our proposed dependable, distributed SHM solution outperforms centralized solution almost in all aspects, including, energy cost of the WSN and offering monitoring system dependability.

REFERENCES

[1] M. Z. A. Bhuiyan, G. Wang, J. Cao, and J. Wu, "Sensor placement with multiple objectives for structural health monitoring," *ACM Transactions on Sensor Networks*, vol. 10, no. 4, pp. 1–45, 2014.

[2] B. Li, D. Wang, F. Wang, and Y. Q. Ni, "High quality sensor placement for SHM systems: Refocusing on application demands," in *Proc. of IEEE INFOCOM*, 2010, pp. 1–9.

[3] S. Olariu and I. Stojmenovic, "Design guidelines for maximizing lifetime and avoiding energy holes in sensor networks with uniform distribution and uniform reporting," in *Proc of IEEE INFOCOM*, 2006, pp. 1–19.
[4] V. Gutnik and A. Chandrakasan, "Embedded power supply for low-power DSP," *IEEE Transactions on VLSI System*, vol. 12, no. 4, pp. 425–434, 1997.
[5] X. Liu, J. Cao, M. Z. A. Bhuiyan, S. Lai, H. Wu, and G. Wang, "Fault tolerant WSN-based structural health monitoring," in *Proc. of IEEE/IFIP DSN'11*, 2011, pp. 37–48.
[6] X. Liu, J. Cao, S. Lai, C. Yang, H. Wu, and Y. Xu, "Energy efficient clustering for WSN-based structural health monitoring," in *Proc. of IEEE INFOCOM*, 2011, pp. 2768–2776.
[7] A. Pandey, M. Biswas, , and M. Samman, "Damage detection from changes in curvature mode shapes," *Journal of Sound and Vibration*, vol. 145, no. 2, p. 1991, 321-332.
[8] F. Perez-Cruz, "Kullback-leibler divergence estimation of continuous distributions," in *Proc. of IEEE ISIT*, 2008, pp. 1666–1670.
[9] Imote2 Hardware Reference Manual, Crossbow Technology Inc. Sep. 2007, PN: 7430-0409-01.